Journal of Clinical Immunology (2019) 39:713–725
https://doi.org/10.1007/s10875-019-00679-4

ORIGINAL ARTICLE

The Phytopathogenic Fungus *Pallidocercospora crystallina*-Caused Localized Subcutaneous Phaeohyphomycosis in a Patient with a Homozygous Missense CARD9 Mutation

Yanyang Guo[1] · Zhenlai Zhu[1] · Jixin Gao[1] · Chen Zhang[1] · Xiujun Zhang[1] · Erle Dang[1] · Wei Li[1,2] · Hongjiang Qiao[1] · Wenjun Liao[1] · Gang Wang[1] · Cuiling Ma[1] · Meng Fu[1]

Received: 18 November 2018 / Accepted: 29 July 2019 / Published online: 14 August 2019

Abstract

Purpose In the past decade, an increasing number of otherwise healthy individuals suffered from invasive fungal infections due to inherited *CARD9* mutations. Herein, we present a patient with a homozygous *CARD9* mutation who was suffering from localized subcutaneous phaeohyphomycosis caused by the phytopathogenic fungus *Pallidocercospora crystallina* which has not been reported to cause infections in humans.

Methods The medical history of our patient was collected. *P. crystallina* was isolated from the biopsied tissue. To characterize this novel pathogen, the morphology was analyzed, whole-genome sequencing was performed, and the in vivo immune response was explored in mice. Whole-exome sequencing was carried out with samples from the patient's family. Finally, the expression and function of mutated *CARD9* were investigated.

Results A dark red plaque was on the patient's left cheek for 16 years and was diagnosed as phaeohyphomycosis due to a *P. crystallina* infection. Whole-genome sequencing suggested that that this strain had a lower pathogenicity. The in vivo immune response in immunocompetent or immunocompromised mice indicated that *P. crystallina* could be eradicated within a few weeks. Whole-exome sequencing revealed ahomozygous missense mutation in *CARD9* (c.1118G>C p.R373P). The mRNA and protein expression levels were similar among cells carrying homozygous (C/C), heterozygous (G/C), and wild-type (G/G) *CARD9* alleles. Compared to PBMCs or neutrophils with heterozygous or wild-type *CARD9* alleles, however, PBMCs or neutrophils with homozygous *CARD9* alleles showed impaired anti-*P. crystallina* effects.

Conclusion Localized subcutaneous phaeohyphomycosis caused by *P. crystallina* was reported in a patient with a homozygous *CARD9* mutation. Physicians should be aware of the possibility of a *CARD9* mutation in seemingly healthy patients with unexplainable phaeohyphomycosis.

Keywords Phaeohyphomycosis · *Pallidocercospora crystallina* · *CARD9* · Homozygous missense mutations · Primary immunodeficiency · Inborn errors of immunity

Introduction

Phaeohyphomycosis covers cutaneous, subcutaneous, and systemic infections caused by a diverse group of darkly pigmented fungi that can be distinguished from other fungal infections by the presence of septate pigmented hyphae or yeast in tissue [1, 2]. Currently, over 100 species of fungi have been identified in the etiology of phaeohyphomycosis [3]. A previous study reported that *Exophiala*, *Fonsecaea*, *Curvularia*, and *Lomentospora* were responsible for most superficial and deep cutaneous phaeohyphomycosis [4, 5]. The distribution of dematiaceous fungi is prevalent worldwide. Surveys for fungal spores in soil or associated plants routinely

Yanyang Guo, Zhenlai Zhu, Jixin Gao and Chen Zhang contributed equally to this work.

Electronic supplementary material The online version of this article (https://doi.org/10.1007/s10875-019-00679-4) contains supplementary material, which is available to authorized users.

✉ Meng Fu
fumeng@fmmu.edu.cn

[1] Department of Dermatology, Xijing Hospital, Fourth Military Medical University, 127 Changlexi Road, Xi'an 710032, Shaanxi, People's Republic of China

[2] Present address: Department of Dermatology, Huashan Hospital, Fudan University, Shanghai 200040, People's Republic of China

detect these molds [6]. *Pallidocercospora crystallina* (its sexual morph is known as *Mycosphaerella crystallina*) belongs to *Pseudocercospora* (its teleomorphic state is known as *Mycosphaerellaceae*) which is the largest group of phytopathogenic fungi [7]. With a widespread distribution, *Pseudocercosporae* usually causes leaf and fruit spots [8] and has not been documented as human pathogen in the literature.

Carbohydrates on the surface of fungi can bind C-type lectin receptors, which are pattern recognition receptor that are predominantly expressed on myeloid cells to initiate antifungal immune responses [9]. The caspase recruitment domain family, member 9 (*CARD9*) encodes a signaling protein that is centrally positioned downstream of many C-type lectin receptors [10]. *CARD9* plays a critical role in the induction of IL-17 responses in fungal infections [11]. The first group of *CARD9* deficiency patients with mucosal and systemic *Candida* infections was described in 2009 [12]. In the past decade, increasing numbers of patients with missense and nonsense *CARD9* mutations have been reported which were associated with the development of a wide spectrum of fungal infections caused by a variety of fungal organisms [13–15]. Most of the patients with deleterious *CARD9* mutations suffered from disseminated or intractable fungal infections [16]. Recently, *CARD9* deficiencies were reported to be associated with subcutaneous phaeohyphomycosis [10, 11, 17, 18].

Herein, we described a patient with subcutaneous phaeohyphomycosis caused by a phytopathogenic fungus, *P. crystallina*, that had not been reported to cause disease in humans. Whole-genome sequencing of the *P. crystallina* and the in vivo immune responses to *P. crystallina* in mice were explored. However, these results cannot explain the subcutaneous phaeohyphomycosis caused by *P. crystallina* in our patient. We speculated that our patient may be immunodeficient. Therefore, whole-exome sequencing of genomic DNA from patient and her parents was performed. Finally, a homozygous missense mutation of *CARD9*, which is deleterious, was identified.

Methods

Fungal Culture and Sequencing

Small pieces of biopsied dermis were seeded onto Sabouraud glucose agar for 2 weeks at 27 °C. In addition, oat meal agar and corn meal agar were also used to characterize the fungi. The colony sizes of *P. crystallina* on Sabouraud glucose agar were recorded at 1 or 2 weeks after culturing, supplemented with or without cycloheximide (actidione) (0.5 mg/ml) at different temperatures, including 27 °C, 35 °C, and 37 °C. The suspension of *P. crystallina* was prepared using saline with a turbidity of 1.0 or 2.0 (DensiCHEK plus, BioMerieux, France). To quantify the colony-forming units (CFUs) of the suspension with 1.0 or 2.0 turbidity, 50 μl of the suspension was extracted and poured into the Sabouraud glucose agar plate for quantification. Then, a series dilution (1:10) of the suspension was used to quantify the CFUs of *P. crystallina*. For *P. crystallina*, a turbidity of 1.0 or 2.0 corresponded to $1.1 \pm 0.1 \times 10^6$ or $1.2 \pm 0.2 \times 10^7$ CFUs per ml, respectively. For higher CFUs of *P. crystallina*, a reduced volume of PBS was added after centrifuging the suspension. Fungal DNA was extracted using an Ezup Fungi DNA Extraction Kit (Sangon Biotech, Shanghai, China). DNA sequences of the actin (partial, GenBank accession number MF135482), elongation factor (EF-1a, MF135483), 18S rRNA (partial, MF135484), and ITS1-5.8S-ITS2 (internal transcribed spacer, ITS, MF135485) regions were amplified by PCR. The total genomic DNA of *P. crystallina* was extracted using the Rapid Fungi Genomic DNA Isolation Kit following the manufacturer's recommendations (Sangon Biotech, Shanghai). Whole-genome sequencing of the fungi was performed with an Illumina HiSeq (Illumina Inc., San Diego, CA, USA). The assembled genome of *P. crystallina* was deposited at DDBJ/ENA/GenBank under the accession number QQNG00000000. The version described in this paper is version QQNG01000000. The Eukaryotic Orthologous Group (KOG), Kyoto Encyclopedia of Genes (KEGG), and Pathogen-Host Interactions database searches were carried out to map the corresponding genes.

Whole-Exome Sequencing and Copy Number Variation

Genomic DNA was isolated from the peripheral blood by alcohol precipitation according to standard procedures. Exome sequencing of the patient and her parents was performed using an IDT xGen Exome Research Panel, followed by sequencing on an Illumina NovaSeq 6000. Allele frequencies of the identified variants were determined in the genome aggregation database 1000 Genomes and the Exome Aggregation Consortium. Polymorphism variants with minor allele frequency > 5%, synonymous mutations, and mutations located within introns were filtered out (the allele frequency cutoff). Chromosomal microarray analysis for copy number variation (low-pass whole-genome sequencing, 0.6×) was performed on the patient and her healthy parents. Copy number variations were classified according to the American College of Medical Genetics and Genomics guidelines, and an in-house bioinformatics data analysis pipeline was used for variant discovery. The identified

homozygous nonsense mutation in exon 8 of *CARD9* was confirmed by standard Sanger sequencing.

For other detailed methods, please see the Supplementary Methods.

Results

Clinical Report

A 35-year-old woman with a medical history of acne from puberty into her 20s presented with a 16-year history of a dark red plaque with several papules on its surface, and this plaque was located on her left cheek (Fig. 1b, 10-30-2013). Her medical history was otherwise unremarkable. The patient reported that 16 years earlier, she had noticed a papule formation in the site of the current lesion after being pierced by a poplar branch. In addition, she recalled squeezing the papule occasionally. The papule slowly increased in size and was resistant to conventional treatments including cryotherapy and antibiotics. Recently, the papules subsequently progressed insidiously into several glossy and discrete papules surrounding the dark red plaque. The findings of routine parameters including blood test and liver function were normal. No peripheral eosinophilia was observed. The absolute eosinophil number was 0.01×10^9/L (normal range 0–0.06×10^9/L). The relative percentage of eosinophils was 0.3% (normal range 0–1.0%). No allergic symptoms were reported in our patient. She was clinically diagnosed with lupus vulgaris, and a biopsy of the lesion was taken.

The skin biopsy specimen showed exuberant epidermal pseudoepitheliomatous hyperplasia with hyperkeratosis and several microabscesses (Fig. 1c). In the dermis, there was a heavily mixed infiltrate, including neutrophils, epithelioid macrophages, lymphocytes, and plasma cells (Supplemental Fig. 1). Notably, deep pigmented septate hyphae and ovoid-shaped yeast were observed from the stratum corneum to the dermis infiltrate (Fig. 1c), especially within and around the necrotic microabscess and multinuclear giant cells. According to the presentation of pigmented fungal elements observed in a histopathological examination, she was finally diagnosed as subcutaneous phaeohyphomycosis. The patient was prescribed with 200 mg itraconazole twice daily and topical oxiconazole cream twice daily (the treatment process is summarized in Fig. 1a). Only mild improvement was observed after 5 months of anti-fungi treatment (Fig. 1b, 3-30-2014). Terbinafine was then used in combination with itraconazole to increase the anti-fungal effects. However, after more than 4 months of treatment, there were still papules on the original site with mild improvement (Fig. 1b, 8-14-2014). The patient reported the discontinuation of oral anti-fungal drugs. Due to the incompliance of the patient with anti-

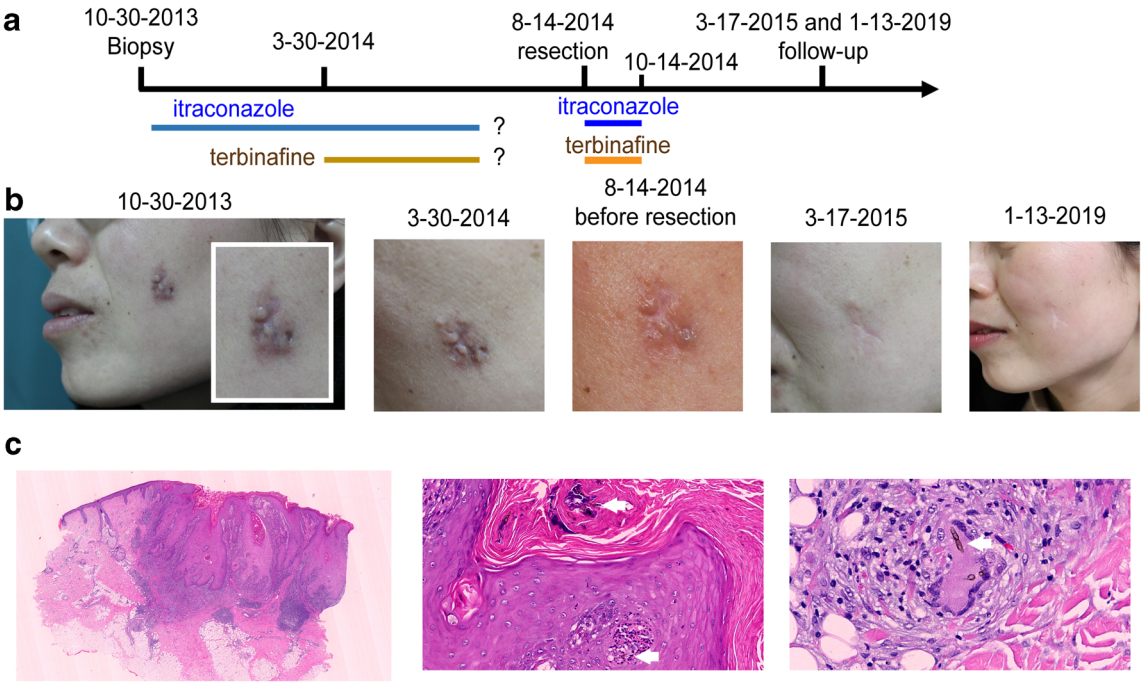

Fig. 1 Clinical course and histological findings of our patient. **a** Treatment process ("?" indicates the discontinuation of the oral terbinafine or itraconazole at an uncertain time) and **b** clinical images during the time course of the disease. **c** Hematoxylin-eosin staining showed epidermal pseudoepitheliomatous hyperplasia and dermis infiltration (original magnification × 12.5). Pigmented hyphae and cigar-shaped yeast in the corneum (white arrow), stratum spinosum (white arrow, original magnification × 200), and multinuclear giant cells in the dermis (white arrow, original magnification × 400) are shown

fungal treatment, surgical excision was performed to remove the entire lesion. After surgery, itraconazole and terbinafine were prescribed for another 2 months to prevent recurrence. A follow-up at 7 months and 4.5 years indicated no evidence of recurrence (Fig. 1b, 3-17-2015 and 1-13-2019).

Identification of the Culprit Fungi with Culturing and DNA Sequencing

Velvety and black colonies were cultured from the excised skin tissue on Sabouraud glucose agar, oat meal agar, or corn meal agar (Fig. 2a, from left to right) after 2 weeks of incubation at 27 °C. To investigate the colony sizes at 27 °C, 35 °C, and 37 °C, the fungi were seeded onto Sabouraud glucose agar with or without cycloheximide supplementation for 2 weeks. As shown in Fig. 2b, at 27 °C, a "volcanic island"-like black colony gradually formed, while only a small (0.4 cm in diameter) black colony formed at 35 °C. Importantly, the fungi were unable to grow at 37 °C. The Sabouraud glucose agar plates with no colony forming at 37 °C were transferred from 37 to 27 °C (Fig. 2c). After transferring, a black colony gradually formed. The results indicate that the isolated fungi can only grow normally at ambient temperature but remain alive at 37 °C. Direct microscopic examination of cultured fungi showed filamentous septate hyphae with pale brown, thickened, wall and no sporulation (Fig. 2d). Furthermore, transmission electron microscopy revealed that connected hyphae were vertically or horizontally fractured because of the easily broken branches (black arrow, Fig. 2e). Due to its nonsporulation on different media, the accurate identification of the fungi at the species level was impossible by morphological methods. Recent advances in molecular techniques have led to the ability to rapidly and accurately identify nonsporulating melanized molds. Therefore, DNA sequences

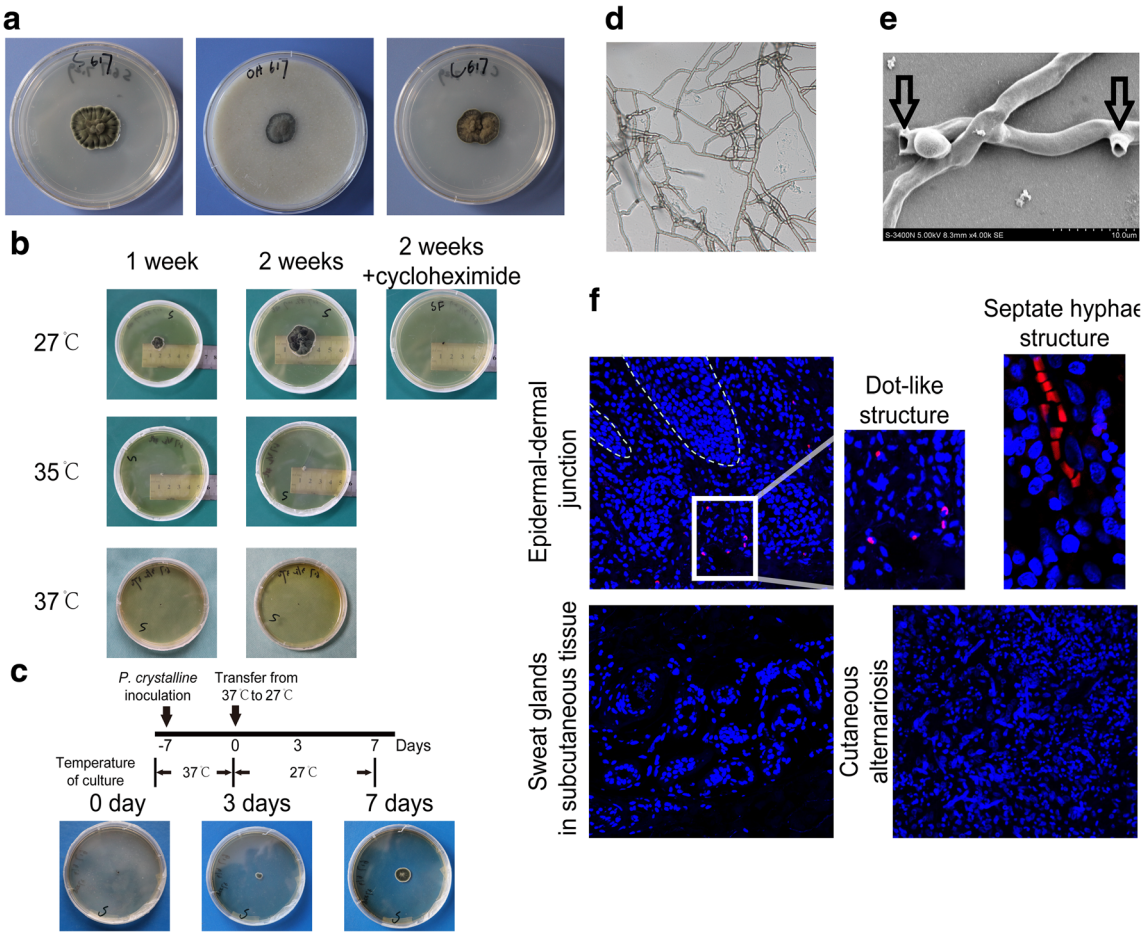

Fig. 2 Identification of the culprit fungus for phaeohyphomycosis in our patient. **a** "Volcanic island"-like black colony on Sabouraud glucose agar, oat meal agar, and corn meal agar (from left to right) after 2 weeks of culture at 27 °C. **b** Colony growth on Sabouraud glucose agar at 27 °C (with or without cycloheximide), 35 °C and 37 °C were recorded for 2 weeks. **c** Colony growth at the indicated time points before and after transferring from 37 °C to 27 °C. **d** Direct microscope examination of cultured fungi revealed septate hyphae without sporulation. **e** Cross-linked hyphae which were easily fractured (arrow) were noted under scanning electron microscopy (original magnification × 4000). **f** *P. crystallina* in shape of a dot-like structure or septate hyphal structure was detected near the epidermal-dermal junction area in the tissue section using in situ fluorescence hybridization (with a cutaneous alternariosis as a control, original magnification × 200)

of the actin (partial), elongation factor, 18S rRNA (partial), and ITS1-5.8S-ITS2 regions were amplified by PCR (GenBank accession numbers MF135482, MF135483, MF135484, MF135485). The sequencing results deposited in GenBank were compared using a basic local alignment search tool (BLAST) search, which identified the *P. crystallina* with a 100% similarity. To exclude the possibility that the isolation of *P. crystallina* from our patient was due to contamination during the biopsy process, fluorescence in situ hybridization (FISH) was performed. As shown in Fig. 2f, a fluorescence probe synthesized according to the ITS sequence of *P. crystallina* can detect the presence of fungi mainly in the superficial dermal area, instead of the deep dermis or subcutaneously where the sweat glands located. Representative images showing probe fluorescence in shape of dot-like or septate hyphae are shown. These results confirmed that *P. crystallina* indeed caused subcutaneous phaeohyphomycosis in our patient.

Whole-Genome Sequencing of *P. crystallina*

The total genomic DNA of cultured *P. crystallina* was extracted. Purified DNA was used to construct an Illumina standard shotgun library with an insert size of 400–500 bp, and then was sequenced using the Illumina HiSeq platform. After sequencing, the raw reads were trimmed and filtered using Trimmomatic-0.36. De novo assembly of short read sequences was performed using the SPAdes Genome Assembler (v.3.5.0), and multi-kmer values were 77, 91, and 127. PrInSeS(G-1.0.0.beta) was utilized to correct these assembled contigs. The assembled 36,958,195 bp genome encoded 15,499 putative coding genes. These putative genes equated to 57.38% of the assembly (1 gene per 2.38 kb). On average, there were 2.17 exons per gene and the average size of protein coding genes was 1368 bp in the genome. The average GC content in the genome was 53%. A total of 45 tRNAs and 27 rRNAs were identified in the *P. crystallina* genome.

The genome was further mapped to the Eukaryotic Clusters of Orthologs (KOG) database to further characterize the putative proteins. A total of 6558 (42.31% of the total predicted genes) protein-coding genes were mapped in the KOG database and were classified into 26 different functional groups (Fig. 3a). The genome contains a large number of putative genes (1727 genes) that were not categorized into a distinct group (categories "General functions prediction only" and "Function unknown"). Apart from the poorly characterized categories, the top three most abundant KOG groups were "Posttranslational modification, protein turnover, and chaperones" (539 genes), "Lipid transport and metabolism" (404 genes), and "Signal transduction mechanisms" (373 genes).

KEGG pathway analysis was carried out to further gain insight into the gene functions in *P. crystallina* (Fig. 3b). A total of 3840 predicted proteins were assigned to their orthologous genes in metabolic pathways in the KEGG database. The top four categories in the KEGG metabolic pathway were carbohydrate metabolism, amino acid metabolism, lipid metabolism, and signal transduction.

The Pathogen-Host Interactions database contains expertly curated molecular and biological information on genes proven to affect the outcome of pathogen-host interactions [19]. Three of top four categories (reduced virulence, unaffected pathogenicity, and the loss of pathogenicity) indicated a lower or unaffected pathogenicity of *P. crystallina* (Fig. 3c).

In Vivo Immune Responses to *P. crystallina* in Mice

To further characterize the pathogenicity of *P. crystallina*, a viable *P. crystallina* suspension was injected subcutaneously into BALB/c, C57BL/6, and ICR mice. Increasing thickness of the footpad, which reflects the local severity of the edema and infiltration, was monitored at the indicated time points. As shown in Fig. 4a, the mouse footpads exhibited peak swelling at 4 days postinfection when the local draining lymph node of the *P. crystallina* injected side was enlarged compared with that of the control side (Fig. 4b). Then, the footpad swelling gradually decreased over 3 to 4 weeks (natural course in Fig. 4c). Among mice with different genetic backgrounds, BALB/c mice showed significantly reduced swelling of footpad comparing to C57BL/6 or ICR mice, which indicates a distinct immune response to *P. crystallina.* Furthermore, heat-killed *P. crystallina* was used to explore whether the swelling of the footpad was attributed to the viability of *P. crystallina.* The same volume of viable or heat-killed *P. crystallina* was subcutaneously injected into the footage of C57BL/6, ICR, or BALB/c mice. One week after infection, compared to the control treatment, heat-killed *P. crystallina* induced a significantly reduced footpad swelling (Fig. 4d). These results suggested that the swelling of the footpad was largely attributed to the viability of *P. crystallina.* Histological examination of the footpads at 1, 3, or 7 days after infection is shown in Fig. 5a. Dematiaceous hyphae were surrounded by large numbers of infiltrating inflammatory cells. Immunofluorescence of mouse Ly6G (Fig. 5b) or myeloperoxidase (Fig. 5c) indicated that neutrophils were predominant in infiltrating cells. The viability of *P. crystallina* after subcutaneous infection was measured using the pan-fungi probe-based qPCR [20]. After the surge of neutrophils into the infectious site, the fungal load of *P. crystallina* sharply decreased (Fig. 5d). Such a short period of elimination suggested that the innate immune response alone may eliminate the *P. crystallina* infection. Neutrophils may play a critical role in the defense of fungal infections [21]. Whether neutrophils play a vital role in the elimination of *P. crystallina* infection was explored using antibody neutralization in vivo (Fig. 5e). Neutrophils were efficiently deleted and examined by flow cytometry using the peripheral blood

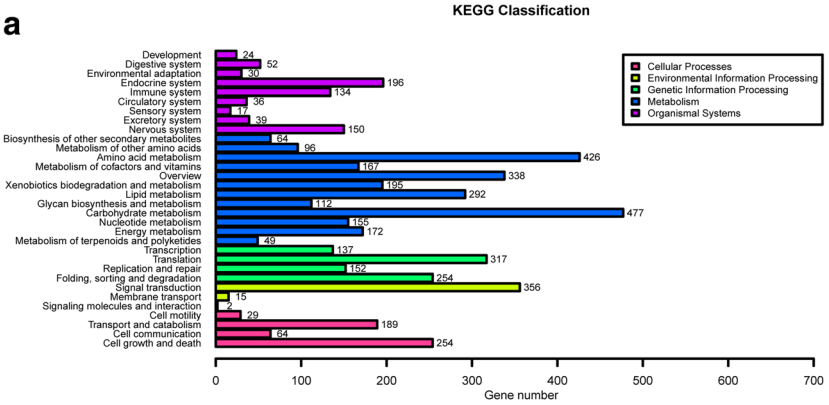
a
KEGG Classification
Development 24
Digestive system 52
Environmental adaptation 30
Endocrine system 196
Immune system 134
Circulatory system 36
Sensory system 17
Excretory system 39
Nervous system 150
Biosynthesis of other secondary metabolites 84
Metabolism of other amino acids 96
Amino acid metabolism 426
Metabolism of cofactors and vitamins 167
Overview 338
Xenobiotics biodegradation and metabolism 195
Lipid metabolism 292
Glycan biosynthesis and metabolism 112
Carbohydrate metabolism 477
Nucleotide metabolism 155
Energy metabolism 172
Metabolism of terpenoids and polyketides 49
Transcription 137
Translation 317
Replication and repair 152
Folding, sorting and degradation 254
Signal transduction 356
Membrane transport 15
Signaling molecules and interaction 2
Cell motility 29
Transport and catabolism 189
Cell communication 64
Cell growth and death 254
Cellular Processes
Environmental Information Processing
Genetic Information Processing
Metabolism
Organismal Systems
0 100 200 300 400 500 600 700
Gene number

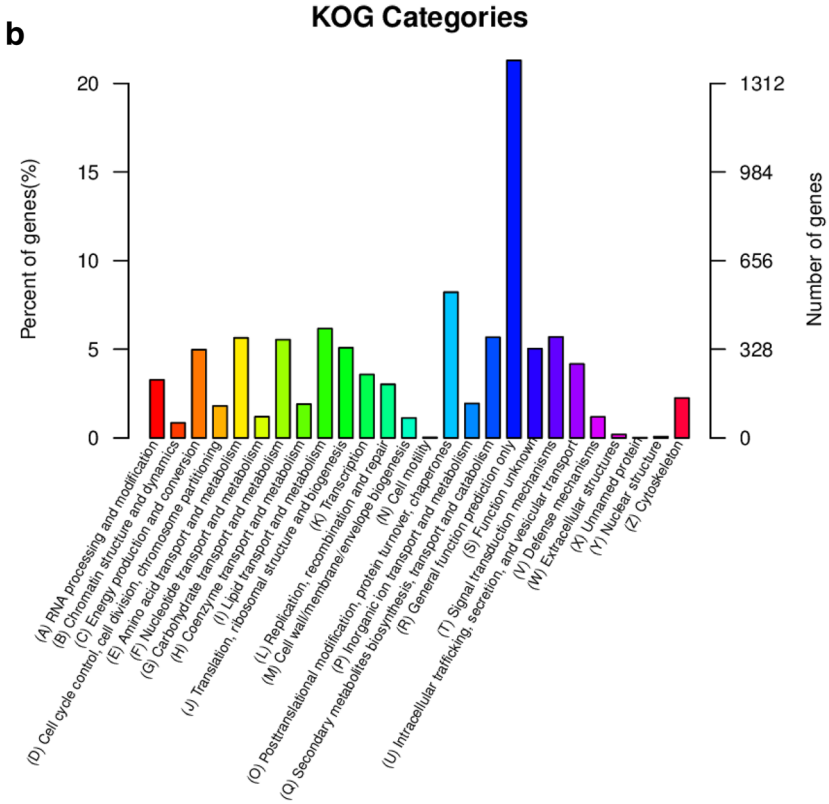
b
KOG Categories
Percent of genes(%)
Number of genes
0 5 10 15 20
0 328 656 984 1312
(A) RNA processing and modification
(B) Chromatin structure and dynamics
(C) Energy production and conversion
(D) Cell cycle control, cell division, chromosome partitioning
(E) Amino acid transport and metabolism
(F) Nucleotide transport and metabolism
(G) Carbohydrate transport and metabolism
(H) Coenzyme transport and metabolism
(I) Lipid transport and metabolism
(J) Translation, ribosomal structure and biogenesis
(K) Transcription
(L) Replication, recombination and repair
(M) Cell wall/membrane/envelope biogenesis
(N) Cell motility
(O) Posttranslational modification, protein turnover, chaperones
(P) Inorganic ion transport and metabolism
(Q) Secondary metabolites biosynthesis, transport and catabolism
(R) General function prediction only
(S) Function unknown
(T) Signal transduction mechanisms
(U) Intracellular trafficking, secretion, and vesicular transport
(V) Defense mechanisms
(W) Extracellular structures
(X) Unnamed protein
(Y) Nuclear structure
(Z) Cytoskeleton

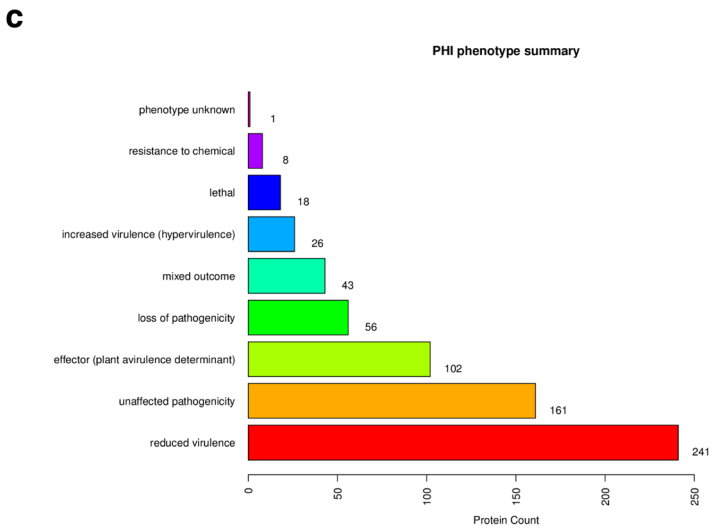
c
PHI phenotype summary
phenotype unknown 1
resistance to chemical 8
lethal 18
increased virulence (hypervirulence) 26
mixed outcome 43
loss of pathogenicity 56
effector (plant avirulence determinant) 102
unaffected pathogenicity 161
reduced virulence 241
0 50 100 150 200 250
Protein Count

◀ **Fig. 3** Whole-genome sequencing of *Pallidocercospora crystallina*. **a** KEGG classifications of genes in the *P. crystallina* genome. **b** KOG class annotation distribution of the *P. crystallina* genome. **c** Pathogen-host interaction annotation of the *P. crystallina* genes

(data not shown). The back skin of the mice was subcutaneously injected with *P. crystallina*, and mice without neutrophils showed significantly increased fungal burdens 5 days after infection (Fig. 5f). Moreover, all neutrophil-depleted mice were survived. No signal was amplified using the pan-fungal probe-based qPCR in the draining popliteal lymph node from the neutrophil-depleted or control mice. In order to further clarify the immune response in vivo, nude mice with a greatly reduced number of T cells leading to an inhibited adaptive immune response were used. As shown in Fig. 5g, nude mice displayed a milder foot thickness compared to that of the immunocompetent mice. However, nude mice eventually eradicated the *P. crystallina* infection. The above results indicate that the innate killing mechanisms of neutrophils alone can effectively eliminate the injected *P. crystallina*. In addition, in mice with the intraperitoneal infection of *P. crystallina*, both immunocompetent mice including BALB/c, C57BL/6, and ICR mice and immunocompromised nude mice were alive and gained weight normally after infection. Four weeks after infection, a histological examination of the spleen, liver, lung, kidney, mesenteric lymph nodes and omentum majus revealed no sign of infection (Supplemental Fig. 2). Moreover, tissues including the spleen, liver, mesenteric lymph nodes, and omentum majus were harvested at 2 weeks after the intraperitoneal infection of *P. crystallina*. Using the pan-fungal probe qPCR, no signal was generated in the DNA extracted from the above tissues. These results indicated both immunocompetent mice including BALB/c, C57BL/6, and ICR mice and immunocompromised nude mice can eliminate an intraperitoneal *P. crystallina* infection.

Whole-Exome Sequencing and Copy Number Variation in the Patient and Her Parents

The short period of elimination of *P. crystallina* infections in mice was inconsistent with the long history of our patient. Therefore, we hypothesized that our patient may carry an inborn error which causes her susceptibility to *P. crystallina* infections. In order to verify our

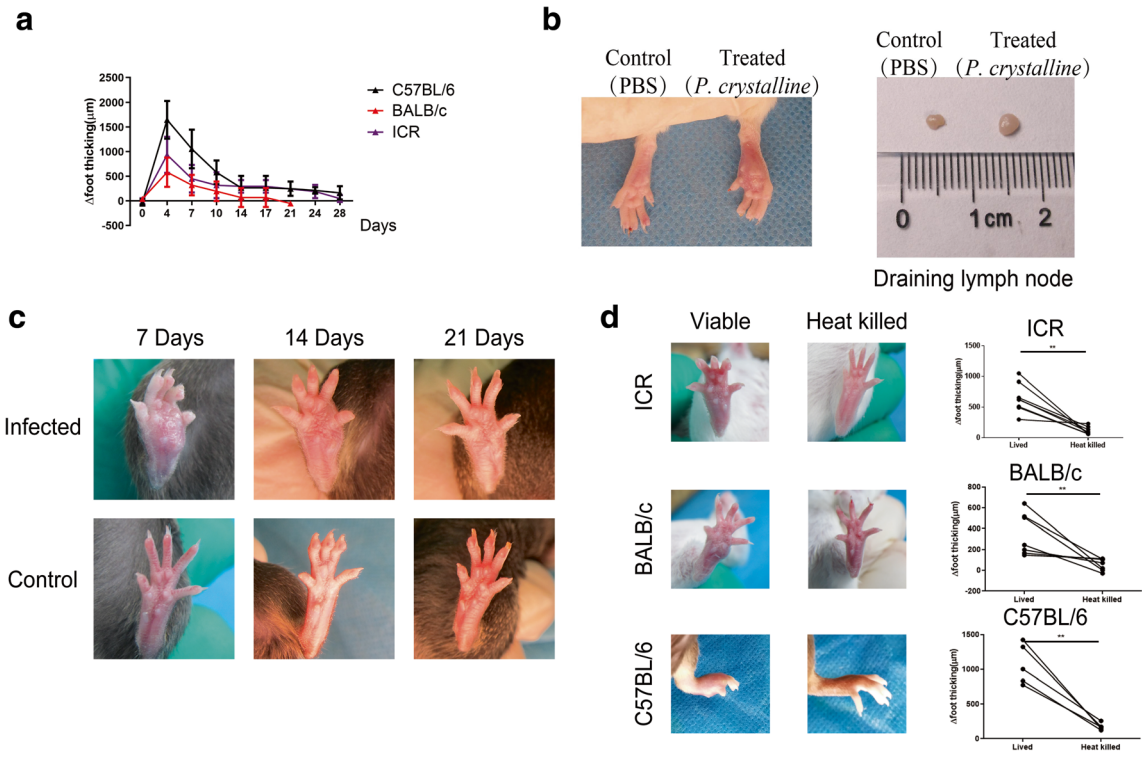

Fig. 4 Different strains of mice can efficiently eliminate subcutaneously injected *Pallidocercospora crystallina*. One side of the hind footpads was subcutaneously injected with 100 μl viable *P. crystallina*. The other side of the hind footpads were subcutaneously injected with 100 μl saline as a control. **a** Foot thickness was measured at the indicated time points after injection into mice with different genetic backgrounds including C57BL/6, BALB/c, and ICR, and the increase in foot thickness from the baseline is shown. **b** Foot lesions and draining lymph nodes from ICR mice are shown 3 days after injection. **c** The time course of subcutaneous *P. crystallina* infection in C57BL/6 mice over 3 weeks. **d** One side of hind footpads was subcutaneously injected with 100 μl viable *P. crystallina.* The other side of the hind footpads was subcutaneously injected with 100 μl heat-killed *P. crystallina.* The increase in foot thickness from the baseline is shown. Data shown is representative of three independent experiments

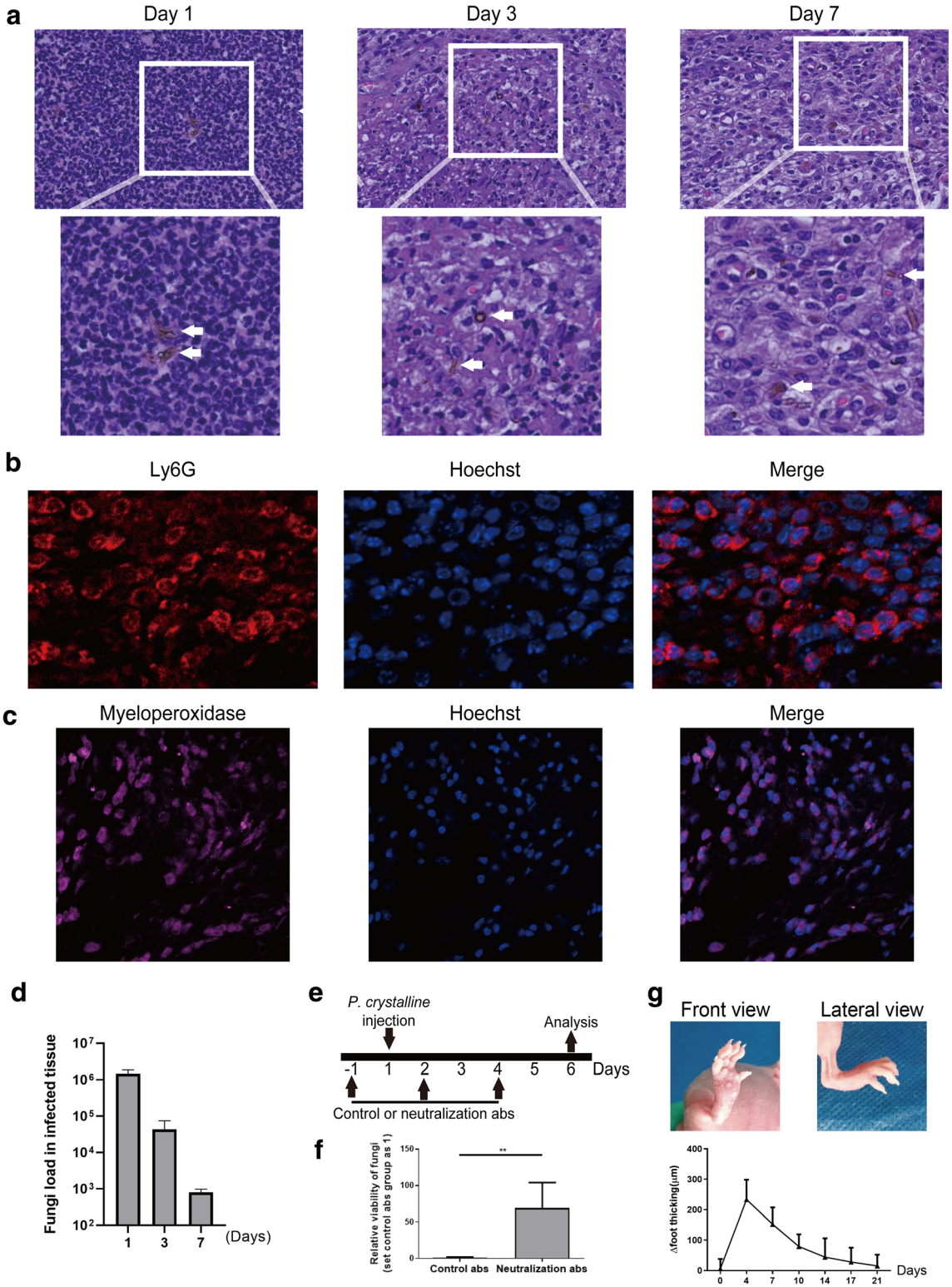

Fig. 5 Neutrophils' role in eliminating *P. crystallina* infection. **a** Hematoxylin-eosin staining tissue sections at 1, 3, and 7 days after the subcutaneous injection of *P. crystallina* into the back skin of mice (white arrow indicates pigmented fungi, original magnification × 200). **b** Ly6G-positive neutrophils are shown in the section 3 days after infection. **c** Myeloperoxidase-positive neutrophils are shown in the section 3 days after infection. **d** The absolute number of fungi in the infected tissues at days 1, 3, or 7 after subcutaneous *P. crystallina* injection. **e** Schematic of the experimental protocol for eliminating the neutrophils. **f** Five days after subcutaneous *P. crystallina* injection into the back skin, the absolute number of fungi was determined and was calculated as the relative fungal viability with the mean of the control group as 1. **g** One week after the subcutaneous injection of *P. crystallina*, the footpads of nude mice and their foot thickness are shown. Data shown is representative of three independent experiments

speculation, whole-exome sequencing of genomic DNA from the patient and her parents was performed and detected a possible homozygous missense mutation in *CARD9* (c. 1118 G>C or p.R373P, Fig. 6a). Copy number variation was otherwise normal in the patient and her parents. Sanger sequencing of *CARD9* in the patient's DNA identified a homozygous missense mutation (Supplemental Fig. 3a), c. 1118 G>C or p.R373P, located in the 8th exon in coiled-coil domain. Homozygosity of the mutation was not present in control databases (1000 Genomes, Exome Aggregation Consortium, or Genome Aggregation Database). The minor allele frequency of this variant was 0.000024 (details are shown in Supplemental Table 1). All the rare and novel homozygous variants seen in the trios are listed in Supplemental Table 1. Notably, the parents were consanguineous. The proband is the offspring of a first cousin union. The parents and the son of our patient were all asymptomatic and heterozygous carriers of the corresponding mutation. Computational analysis of the c. 1118 G>C indicated possibly damaging or deleterious, which was reported in a recent review [15]. Consistent with this, patients with an autosomal recessive *CARD9* deficiency have been shown to predispose them to increased susceptibility to fungal infections in a recent decade [22, 23]. The mutations cluster in the two functional domains of *CARD9* (Supplemental Fig. 4). Several types of mutations in *CARD9* have been identified which range from loss of expression (L64fs*59, Q158X, D274fs*60, Q289X, Q295X, and E323del) to the loss of function (R57H, R70W, G72S, Y91H, R101C, and R373P). In order to investigate the expression and function of mutated *CARD9*, peripheral blood from the patient, the son of the patient and three unrelated healthy controls were collected. Sanger sequencing of *CARD9* using the peripheral blood DNA identified a heterozygous c. 1118 G>C in the son of the patient, while the three healthy controls harbored wild-type alleles (Supplemental

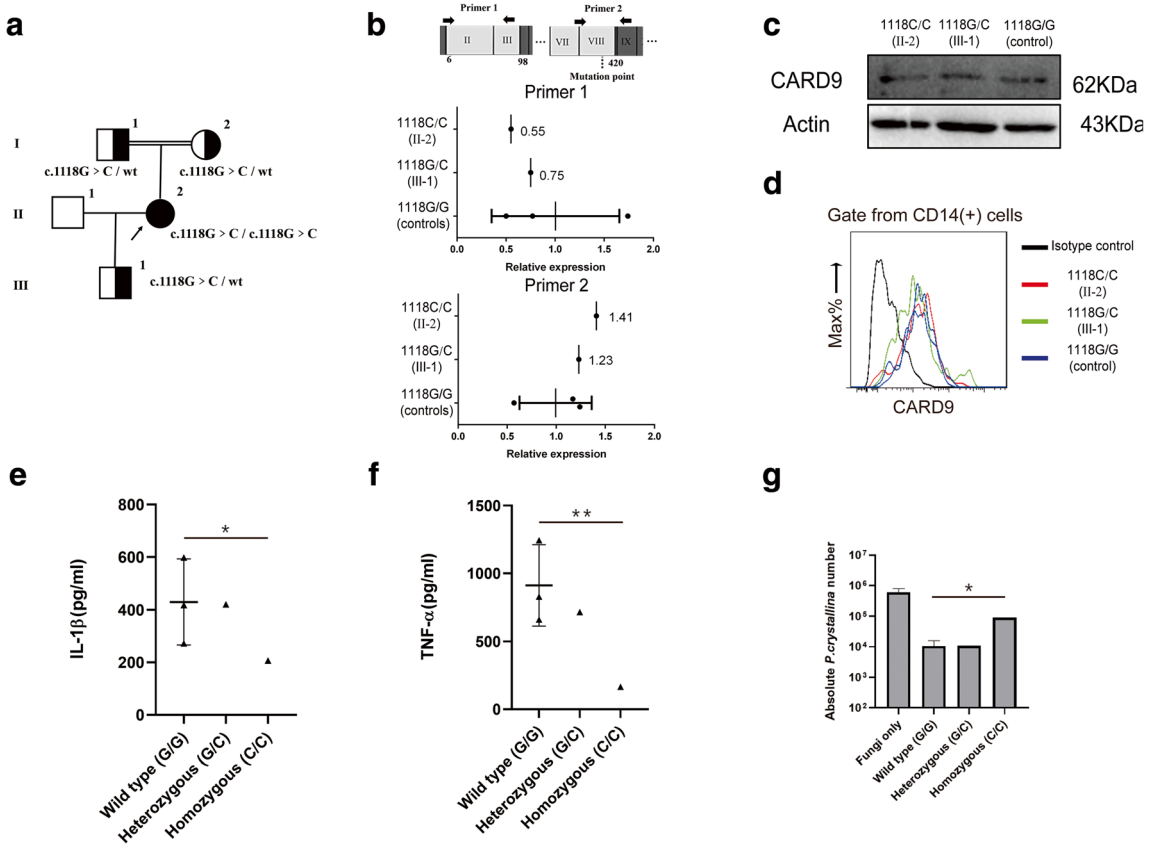

Fig. 6 Deleterious homozygous missense mutations of *CARD9* in our patient. **a** Pedigree analysis, with the genotype of family members. **b** Relative mRNA expression levels of CARD9 using two primers. **c** Protein expression of CARD9 was measured in leukocytes carrying homozygous, heterozygous and wild-type alleles by a western blot. **d** Flow cytometry analysis of CARD9 expression gated from the CD14-positive cells in the PBMCs. **e** IL-1β and **f** TNF-α production by wild-type (G/G), heterozygous (G/C), or homozygous (C/C) CARD9 PBMCs after 24 h of stimulation with *P. crystallina*. **g** The absolute number of *P. crystallina* after 24-h coculture of neutrophils carrying wild-type, heterozygous, or homozygous CARD9 with *P. crystallina* in vitro. The experiment using the peripheral blood from the patient, the patient's son and three unrelated healthy controls was done for one time due to the limited number of cells. Single asterisks (*) indicate $P < 0.05$ and double asterisks (**) indicate $P < 0.01$

Fig. 3b). The mRNA expression of *CARD9* was similar among the patient, the son of the patient, and the three unrelated controls (Fig. 6b). The protein expression of *CARD9* was evaluated by a western blot (Fig. 6c) and flow cytometry (Fig. 6d) and indicated that different alleles expressed similar levels of *CARD9*. These results indicate that the homozygous c. 1118 G>C mutation may not alter the expression of the *CARD9* protein. To investigate whether mutated *CARD9* leads to impaired anti-*P. crystallina* function, responses to *P. crystallina* were evaluated by the production of IL-1β and TNF-α in the supernatants after the coculture of PBMCs with *P. crystallina.* As shown in Fig. 6e–f, the production of TNF-α or IL-1β was significantly decreased in peripheral blood mononuclear cells (PBMCs) carrying homozygous mutations (the patient, 1118C/C) comparing to the heterozygous (the son of the patient, 1118G/C) or wild-type (three healthy controls, 1118G/G) controls. Furthermore, the anti-*P. crystallina* ability of neutrophils were also explored using the coculture of neutrophils with *P. crystallina.* After 24 h of coculture, the DNA was extracted from the sediment of each well for the quantification of the absolute number of fungi using the pan-fungal probe-based method (Fig. 6g). The results indicate that, compared to that in heterozygous or wild-type neutrophils, the anti-*P. crystallina* activity was significantly reduced in the patient's neutrophils. Collectively, these data strongly suggest that our patient is homozygous for a deleterious mutant *CARD9* allele.

Discussion

Phaeohyphomycosis, which refers to a group of infections caused by dematiaceous fungi, can be divided into superficial, subcutaneous, and systematic types from a variety of genera [5, 24]. Although the patient is often unaware of it, the disease is often associated with traumatic implantation on exposed areas of the body. In the current case, our patient reported that she had been punctured by a poplar branch on her face, but it is difficult to ascertain if this incident is related to her phaeohyphomycosis. Moreover, presentation is usually indolent, with the mass or cyst gradually enlarging for weeks to months. Currently, no standard treatment has been established for phaeohyphomycosis. Oral anti-fungal agents such as itraconazole and terbinafine are frequently used [4]. However, there was mild improvement without eradication in our patient after oral itraconazole and terbinafine treatment, which may be due to the discontinuation of antifungal drugs. Moreover, localized phaeohyphomycosis can also be treated with excision. In our patient, surgical excision successfully removed the lesion without recurrence at the 4.5-year follow-up.

New fungal species have been increasingly reported as pathogenic fungal species in phaeohyphomycosis, especially with the help of molecular tools [5]. The reproductive structures and the conidia are required for identification of molds under a microscope. However, for nonsporulating molds, such as *P. crystallina* in our case, the species identification heavily relies on molecular tools. Consistent with our observations, Feng et al. reported that *P. crystallina* isolated from the spot leaves of citrus cannot be induced to sporulate [8]. Therefore, the identification of pathogenic nonsporulating fungi by morphological means is extremely difficult, which highlights the importance of molecular techniques in the diagnosis of this disease. In addition, a previous study [25] reported that molecular tools can provide a fast and accurate identification of fungi at the species level for filamentous molds, which can guide the treatment of fungal infections. *Pseudocercospora* species are well known as plant pathogens for important food crops and other plants. DNA phylogenetic analysis showed that *Pseudocercospora* is heterogeneous and contains hundreds of species. *P. crystallina* was first isolated from the leaves of *Eucalyptus bicostata* in 1996 by Crous and M. J Wingf [7]. Moreover, *Pseudocercospora* was isolated from lichens as plant-inhabitants without pathogenic phenomena [26]. In a recent study, *P. crystallina* was also isolated from *Citrus* in China [8]. However, a detailed description of this fungus is absent and the whole genome sequencing of *P. crystallina* in our study provided insights into the features of *P. crystallina.*

Neutrophils are critical for eliminating invasive fungal infections. As the most numerous cellular soldiers in the blood, neutrophils are recruited into the skin lesion with an arsenal of antimicrobial agents after a fungal infection. A histological examination of our patient revealed several small neutrophil microabscesses surrounding the pigmented fungi. Consistent with this finding, histological analyses of the skin from three patients with subcutaneous phaeohyphomycosis revealed a lack of neutrophil infiltration. However, whether the local lesion of our patient can recruit a number of neutrophils comparable to that in wild-type individuals requires further investigation. Due to the long duration of the disease, multinuclear giant cells were generated to combat fungal infection. This is often observed in chronic cutaneous infections. Several previous studies reported that neutrophils from patients with CARD9 mutation showed defective killing ability of different fungi [27–29]. Even though the reduced anti-*P. crystallina* ability of the neutrophils from the patient was observed in vitro, neutrophils from the patient can also lower the fungal burden after 24-h coculture. One hypothesis is that during the 16-year period of the *P. crystallina* infection, neutrophils would be recruited

continuously into the lesion to eradicate *P. crystallina*. However, in contrast to the massive neutrophil infiltration in *P. crystallina* infected mice, only a limited number of neutrophils were observed in the lesion of our patient. Such a limited number of neutrophils may be insufficient to eradicate *P. crystallina* infection. Therefore, whether the local lesion of the patient can recruit a number of neutrophils comparable to that recruited by wild-type individuals requires further investigation. Moreover, the neutrophil recruitment into the fungus-infected sites maybe tissue-, mutation-, and fungal-specific. Recent study indicated that neutrophil recruitment was significantly reduced in microglia-specific *CARD9* deletion in a central nervous system fungus infection model induced by *Candida albicans* [27, 30]. Whether the recruitment of neutrophils was impaired in our patient needs further exploration. In addition, the underlying microbicidal mechanism of neutrophils may involve the neutrophil extracellular traps [31] and the neutrophil-dendritic cell hybrid [32] in antifungal immunity [27, 33].

The *CARD9* gene encodes a protein of 536 amino acids which contains an N-terminal CARD domain and a C-terminal coiled-coil domain. A recent review [15] summarized that most of the patients with *CARD9* mutation showed impaired IL-1β and TNF-α production by PBMCs, excepts for patients harboring Y91H *CARD9* mutation [34, 35]. The cytokines IL-1β and TNF-α have a wide spectrum of biological activities and are essential for the differentiation of Th17 cells. Insufficient IL-1β and TNF-α by PBMCs after *P. crystallina* stimulation in our patient may play a role in the pathogenesis of *P. crystallina*-caused phaeohyphomycosis. Increasing numbers of patients with *CARD9* mutations who suffered from intractable or disseminated fungal infections have been reported in the last decade. Moreover, most patients with *CARD9* mutations experienced relapses of fungal infection when treatment was stopped [15]. However, the localized phaeohyphomycosis caused by *P. crystallina* in our patient was not disseminated during the 16-year history of infection. Furthermore, our patient remained healthy at 4.5 years after lesion resection. On the one hand, these phenomena may be attributed to the inhibitory effect of core body temperature (35 to 37 °C) on the growth of *P. crystallina*. However, the homozygous mutation in the 8th exon in the coiled-coil domain may only partially affect the function of the *CARD9* protein. A previous study reported invasive fungal meningoencephalitis due to a compound heterozygote mutation of *CARD9* (G72S and R373P) [28]. Since the G72S mutation was located in the CARD domain, the homozygous mutation in the coiled-coil domain in our patient may generate different deleterious effects. In contrast to the CARD domain which can mediate binding with other molecules, the C-terminal coiled-coil domain enables protein oligomerization. Previous studies have reported that spontaneous *Candida* infections of the central nervous system in patients with homozygous *CARD9* missense mutations (R57H or Y91H) respond differently to recombinant granulocyte-macrophage colony-stimulating factor treatment [27, 35, 36]. These results indicate that the underlying mechanisms may be disparate due to mutations at different *CARD9* gene loci. In addition, not all amino acid changes in *CARD9* influence the individuals' susceptibility to fungal infections. For example, no significant association between the single-nucleotide polymorphisms *CARD9* S12N and the prevalence of candidemia or recurrent vulvovaginal candidiasis was found [23, 37]. However, *CARD9* S12N promotes the production of IL-5 from alveolar macrophages and facilitates the type 2 immune responses [38]. Therefore, whether there are functional differences in *CARD9* mutations between this homozygous mutation and other devastating *CARD9* mutations needs further investigation.

In conclusion, our case suggests that *Pseudocercospora*, a group of well-known phytopathogenic fungi, may also have pathogenicity in humans with *CARD9* mutations. When phaeohyphomycosis presents with multiple or polymorphous lesions [39, 40] or is caused by a relatively rare fungus [41, 42] that was encountered by a seemingly immunocompetent individual, physicians should examine the patient for underlying *CARD9* mutations.

Acknowledgments We thank the patient and her family, for participating in this study. We thank for the Chigene (Beijing) Translational Medical Research Center Co. Ltd. for the technical support of the whole-exome sequencing analysis.

Authors' Contributions Y.G., Z.Z, J.G., C.Z., X.Z., E.D., W.L., and H.Q. conducted the research, analyzed, and interpreted data. G.W., C.M., and M.F. designed the research studies. Y.G., Z.Z., and J.G. drafted the manuscript and E.D., W.L., H.Q., G.W., C.M., and M.F. critically revised the manuscript.

Funding This work was supported by the National Natural Science Foundation of China (Grant numbers 81371735 and 81672691) and the National Natural Science Foundation of Shaanxi Province (Grant number 21044091).

Compliance with Ethical Standards

This work was performed according to rules and regulations concerning the use of human materials from the patient, her parents, her son, and three healthy unrelated volunteers with written informed consent. The study was approved by the Clinical Research Ethics Committee of the Xijing Hospital in accordance with the institution's guidelines. All experiments were carried out with adherence to the Declaration of Helsinki.

Conflict of Interest The authors declare that they have no conflicts of interest.

References

1. Chowdhary A, Perfect J, de Hoog GS. Black molds and melanized yeasts pathogenic to humans. Csh Perspect Med. 2015;5(8): a19570.
2. Skupsky H, Junkins-Hopkins J. Counterfeit pennies: distinguishing chromoblastomycosis from phaeohyphomycotic infections. Am J Dermatopathol. 2017;39(6):485–7.
3. Kollipara R, Peranteau AJ, Nawas ZY, Tong Y, Woc-Colburn L, Yan AC, et al. Emerging infectious diseases with cutaneous manifestations. J Am Acad Dermatol. 2016;75(1):19–30.
4. Revankar SG, Baddley JW, Chen SCA, Kauffman CA, Slavin M, Vazquez JA, et al. A Mycoses Study Group international prospective study of phaeohyphomycosis: an analysis of 99 proven/probable cases. Open Forum Infect Di. 2017;4(4).
5. Isa-Isa R, García C, Isa M, Arenas R. Subcutaneous phaeohyphomycosis (mycotic cyst). Clin Dermatol. 2012;30(4): 425–31.
6. Wong EH, Revankar SG. Dematiaceous molds. Infect Dis Clin N Am. 2016;30(1):165–78.
7. Crous PW, Braun U, Hunter GC, Wingfield MJ, Verkley GJ, Shin HD, et al. Phylogenetic lineages in Pseudocercospora. Stud Mycol. 2013;75(1):37–114.
8. Huang F, Groenewald JZ, Zhu L, Crous PW, Li H. Cercosporoid diseases of Citrus. Mycologia. 2016;107(6):1151–71.
9. Tang J, Lin G, Langdon WY, Tao L, Zhang J. Regulation of C-type lectin receptor-mediated antifungal immunity. Front Immunol. 2018;9.
10. Wang X, Zhang R, Wu W, Song Y, Wan Z, Han W, et al. Impaired specific antifungal immunity in CARD9-deficient patients with phaeohyphomycosis. J Invest Dermatol. 2018;138(3):607–17.
11. Wang X, Wang W, Lin Z, Wang X, Li T, Yu J, et al. CARD9 mutations linked to subcutaneous phaeohyphomycosis and TH17 cell deficiencies. J Allergy Clin Immunol. 2014;133(3):905–8.
12. Glocker E, Hennigs A, Nabavi M, Schäffer AA, Woellner C, Salzer U, et al. A Homozygous CARD9 mutation in a family with susceptibility to fungal infections. N Engl J Med. 2009;21(4):372.
13. Gavino C, Mellinghoff S, Cornely OA, Landekic M, Le C, Langelier M, et al. Novel bi-allelic splice mutations in CARD9 causing adult-onset Candida endophthalmitis. Mycoses. 2018;61(1):61–5.
14. Sari S, Dalgic B, Muehlenbachs A, DeLeon-Carnes M, Goldsmith CS, Ekinci O, et al. Prototheca zopfii colitis in inherited CARD9 deficiency. J Infect Dis. 2018;218(3):485–9.
15. Corvilain E, Casanova J, Puel A. Inherited CARD9 deficiency: invasive disease caused by ascomycete fungi in previously healthy children and adults. J Clin Immunol. 2018;38(6):656–93.
16. Rieber N, Gazendam RP, Freeman AF, Hsu AP, Collar AL, Sugui JA, et al. Extrapulmonary Aspergillus infection in patients with CARD9 deficiency. JCI Insight. 2016;1(17).
17. Yan XX, Yu CP, Fu XA, Bao FF, Du DH, Wang C, et al. CARD9 mutation linked to Corynespora cassiicola infection in a Chinese patient. Brit J Dermatol. 2016;174(1):176–9.
18. Arango-Franco CA, Moncada-Vélez M, Beltrán CP, Berrío I, Mogollón C, Restrepo A, et al. Early-onset invasive infection due to Corynespora cassiicola associated with compound heterozygous CARD9 mutations in a Colombian patient. J Clin Immunol. 2018;38(7):794–803.
19. Urban M, Pant R, Raghunath A, Irvine AG, Pedro H, Hammond-Kosack KE. The Pathogen-Host Interactions database (PHI-base): additions and future developments. Nucleic Acids Res. 2015;43(D1):D645–55.
20. Miyajima Y, Satoh K, Uchida T, Yamada T, Abe M, Watanabe S, et al. Rapid real-time diagnostic PCR for Trichophyton rubrum and Trichophyton mentagrophytes in patients with tinea unguium and tinea pedis using specific fluorescent probes. J Dermatol Sci. 2013;69(3):229–35.
21. Gazendam RP, van de Geer A, Roos D, van den Berg TK, Kuijpers TW. How neutrophils kill fungi. Immunol Rev. 2016;273(1):299–311.
22. Lanternier F, Pathan S, Vincent QB, Liu L, Cypowyj S, Prando C, et al. Deep dermatophytosis and inherited CARD9 deficiency. N Engl J Med. 2013;369(18):1704–14.
23. Rosentul DC, Plantinga TS, Oosting M, Scott WK, Velez Edwards DR, Smith PB, et al. Genetic variation in the dectin-1/CARD9 recognition pathway and susceptibility to candidemia. J Infect Dis. 2011;204(7):1138–45.
24. Revankar SG, Sutton DA. Melanized fungi in human disease. Clin Microbiol Rev. 2010;23(4):884–928.
25. Santos DWCL, Padovan ACB, Melo ASA, Gonçalves SS, Azevedo VR, Ogawa MM, et al. Molecular identification of melanised non-sporulating moulds: a useful tool for studying the epidemiology of phaeohyphomycosis. Mycopathologia. 2013;175(5–6):445–54.
26. Harutyunyan S, Muggia L, Grube M. Black fungi in lichens from seasonally arid habitats. Stud Mycol. 2008;61:83–90.
27. Drummond RA, Collar AL, Swamydas M, Rodriguez CA, Lim JK, Mendez LM, et al. CARD9-dependent neutrophil recruitment protects against fungal invasion of the central nervous system. Plos Pathog. 2015;11(12):e1005293.
28. Drewniak A, Gazendam RP, Tool AT, van Houdt M, Jansen MH, van Hamme JL, et al. Invasive fungal infection and impaired neutrophil killing in human CARD9 deficiency. Blood. 2013;121(13): 2385–92.
29. Liang P, Wang X, Wang R, Wan Z, Han W, Li R. CARD9 deficiencies linked to impaired neutrophil functions against Phialophora verrucosa. Mycopathologia. 2015;179(5–6):347–57.
30. Drummond RA, Swamydas M, Oikonomou V, Zhai B, Dambuza IM, Schaefer BC, et al. CARD9(+) microglia promote antifungal immunity via IL-1beta- and CXCL1-mediated neutrophil recruitment. Nat Immunol. 2019;20(5):559–70.
31. Johnson CJ, Davis JM, Huttenlocher A, Kernien JF, Nett JE. Emerging fungal pathogen Candida auris evades neutrophil attack. Mbio. 2018;9(4).
32. Fites JS, Gui M, Kernien JF, Negoro P, Dagher Z, Sykes DB, et al. An unappreciated role for neutrophil-DC hybrids in immunity to invasive fungal infections. Plos Pathog. 2018;14(5):e1007073.
33. Drummond RA, Franco LM, Lionakis MS. Human CARD9: a critical molecule of fungal immune surveillance. Front Immunol. 2018;9.
34. Gavino C, Hamel N, Zeng JB, Legault C, Guiot MC, Chankowsky J, et al. Impaired RASGRF1/ERK-mediated GM-CSF response characterizes CARD9 deficiency in French-Canadians. J Allergy Clin Immunol. 2016;137(4):1178–88.
35. Gavino C, Cotter A, Lichtenstein D, Lejtenyi D, Fortin C, Legault C, et al. CARD9 deficiency and spontaneous central nervous system candidiasis: complete clinical remission with GM-CSF therapy. Clin Infect Dis. 2014;59(1):81–4.
36. Drummond RA, Zahra FT, Natarajan M, Swamydas M, Hsu AP, Wheat LJ, et al. GM-CSF therapy in human caspase recruitment domain–containing protein 9 deficiency. J Allergy Clin Immunol. 2018;142(4):1334–8.
37. Rosentul DC, Delsing CE, Jaeger M, Plantinga TS, Oosting M, Costantini I, et al. Gene polymorphisms in pattern recognition receptors and susceptibility to idiopathic recurrent vulvovaginal candidiasis. Front Microbiol. 2014;5.
38. Xu X, Xu J, Zheng G, Lu H, Duan J, Rui W, et al. CARD9S12N facilitates the production of IL-5 by alveolar macrophages for the induction of type 2 immune responses. Nat Immunol. 2018;19(6): 547–60.

39. Behera B, Thomas E, Kumari R, Thappa DM, Jinkala S. Polymorphous presentation of subcutaneous phaeohyphomycosis: a rare occurrence. Int J Dermatol. 2018;57(2):e1–3.
40. Zhou YB, Chen P, Sun TT, Wang XJ, Li DM. Acne-like subcutaneous Phaeohyphomycosis caused by Cladosporium cladosporioides: a rare case report and review of published literatures. Mycopathologia. 2016;181(7–8):567–73.
41. Yang H, Cai Q, Gao Z, Lv G, Shen Y, Liu W, et al. Subcutaneous phaeohyphomycosis caused by Exophiala oligosperma in an immunocompetent host: case report and literature review. Mycopathologia. 2018.
42. Mijiti J, Pan B, de Hoog S, Horie Y, Matsuzawa T, Yilifan Y, et al. Severe chromoblastomycosis-like cutaneous infection caused by Chrysosporium keratinophilum. Front Microbiol. 2017;8.